High Resolution Weather Forecast Over Complex Orography: Sensitivity to the Assimilation of Conventional Data

CLAUDIA FACCANI[1], ROSSELLA FERRETTI[1,2], GUIDO VISCONTI[1,2]
[1] *CETEMPS, Center for the Forecast of Severe Weather by Remote Sensing and Numerical Modelling*
[2] *Department of Physics, University of L'Aquila, Coppito-L'Aquila, Italy*

Accepted by: *Monthly Weather Review* June 2002

Corresponding Author: C. Faccani, e-mail: claudia.faccani@aquila.infn.it

ABSTRACT
Weather forecast over regions with complex orography, as the Alps, presents several problems and the task becomes even more difficult when high resolution is required. Moreover for the Alpine region, some of the problems are due to the lack of observations especially over the Mediterranean sea. A possibility to improve the forecast is to re-use assimilation techniques locally. In this paper we present results obtained through data assimilation: Objective Analysis (OA) of observations and data analyses from the European Center for Medium-Range Weather Forecast (ECMWF) are blended together to generate a new set of meso-scale Initial (I.C.) and Boundary Conditions (B.C.). In particular, OA is applied to surface data and radiosoundings using two methods: Cressman and Multiquadric. The sensitivity of the weather forecast to the number of upper-air stations assimilated by OA is tested using the Piedmont flood (4-6 November 1994). At first, a comparison is made between I.C., obtained through the data assimilation, and the surface data; then a few weather forecast experiments, using the MM5 (PSU/NCAR), are performed to assess the impact of the data assimilation on the forecast. The results show a measurable improvement in the high-resolution precipitation forecast. It is also shown that this technique can be used for high resolution real-time forecasts.

1 Introduction

In the last few years considerable efforts have been devoted to the understanding and forecast of heavy precipitation. The Mesoscale Alpine Programme (MAP) is part of this effort as well as the field campaign organized in its framework. The first phase of the MAP experiment was focused on the improvement of the model simulations through inter-comparison and on the study of the mechanism of Alpine precipitation (Buzzi et al., 1999, Ferretti et al., 2000, Massacand et al., 1998, Richard et al., 1998, etc.). The results obtained during this first phase (1994-1999) aim to show that it would be possible to improve the weather forecast errors for severe events like the Piedmont flood (4-6 November 1994). In this paper this is accomplished by using the Data Assimilation (DA): *Objective Analysis* (OA) (Cressman 1959, Benjamin and Seaman 1985, Nuss and Titley 1994) of the observations and European Center for Medium-Range Weather Forecast (ECMWF) analyses have been used together to produce a new set of mesoscale Initial (I.C.) and Boundary Conditions (B.C.). OA of the observations, surface pressure and upper-air data, is used to correct the meteorological variables. The corrections depend on the distance between each grid point and the recording station and on the difference between the observation and the variable. Usually, the I.C. of a Limited Area Model (LAM) are computed by interpolating the data analyses from the large scale to the small one. This technique does not guarantee a good response, especially for the high resolution forecast over areas where the orography presents strong horizontal and vertical gradients. Therefore, the observations and the ECMWF analyses are used to produce a new

data set of I.C. and/or B.C. with the aim to enhance the mesoscale circulation that, otherwise, may be missed by the regular data analyses. The ECMWF analyses used for this study are produced operationally, by running 4DVAR (Four-Dimensional Variational Data Assimilation). To explain such a complex processes, these analyses are the final result of a DA cycle, schematically composed by the following: the Objective Analysis which composes scattered observations into a regular grid; the data-assimilation which aims at combining the model first-guess and OA; the initialization which imposes a dynamic balance between mass and wind fields. These three steps are combined into one by using 4DVAR (Rabier et al., 1998). A review of Data Assimilation techniques is beyond the intent of this paper and the interested readers may refer to Lorenc (1986) and Ghil and Malanotte-Rizzoli (1991). Furthermore, an excellent overview can be found in Daley (1991). The first two steps of DA are already used by ECMWF, but in this study OA is applied at higher resolution than ECMWF, and the analyses are used as First Guess (FG). In the past, a few attempts to improve weather forecast have been done by using observations through FDDA (Four Dimensional Data Assimilation) in a limited area model (Stauffer and Seaman, 1990), associated with a Newtonian relaxation (nudging) technique. The results showed a strong impact for cases dominated by large scale forcing. However, for cases dominated by small-scale convection, FDDA showed only minor improvement in the rainfall. The same technique was also applied for the assimilation of non-conventional data, such as precipitable water, from an hypothetical network of systems measuring water vapor (Kuo et al., 1993). The results showed an improvement of the precipitation forecast. Another study (Stauffer and Seaman, 1994) based on the assimilation of non-conventional data such as Doppler Sodar and Profiler was performed using FDDA (nudging). In this case, the results showed that there are advantages in using asynoptic data depending on the grid size. Direct assimilation of the observations on a fine scale may influence negatively the stability of the model. A study by Schraff (1997) showed that it is possible to improve the forecast of low-stratus on the Alpine region using surface and upper-air data, through nudging technique. It is well known that a good forecast depends on both the quality of the I.C. and the parameterizations used by the model (Bengston, 1978, 1981 and Lorenz, 1982), therefore the approach used for this study is to improve the quality of the mesoscale I.C. and B.C. by DA. The technique used is simple and computationally not expensive. DA is used with the intent to improve the forecast of the 4-6 November 1994 Piedmont flood and a few experiments are described in the next sections. Previous work by Ferretti et al., (2000) showed that the MM5 model could produce a good precipitation forecast over the Piedmont area (Fig.1). However, the comparison with a few other model simulations (Richard et al., 1998) showed a poor skill by the MM5 on the precipitation forecast over the Mediterranean area and on the sea side, particularly where no observations were available. A general underestimation of the light precipitation was found, whereas the heavy precipitation over the Piedmont area was well reproduced. The poor skill in the precipitation forecast may be related to a lack of the mesoscale information

in the I.C. and it is well known that a forecast critically depends on them. Furthermore, Rotunno and Ferretti (2001) showed that this event was driven by large scale forcing, as well as by a strong convergence area over the western Po Valley, related to a strong horizontal gradient of the water vapor content at a low-level. The MM5 results showed that the location of the precipitation was strongly related to the convergence, suggesting that the information on the mesoscale circulation might be a key parameter for a good forecast. Therefore, an attempt is made to improve the mesoscale I.C. of this event by using DA. Two different schemes are tested for OA, and the sensitivity to the choice of different parameters is assessed. The re-assimilation of surface and upper air data within the ECMWF analyses enables the attribution of different wheigt (at higher resolution) to the local information. Furthermore, the experiments performed in this study start 12h before the event, allowing for the model to dynamically adjust, if any unbalanced flow should occur. In section 2 a brief description of the meteorological situation of the Piedmont case is presented. In section 3 and 4, the OA schemes and the impact of the DA on the I.C. are discussed. The description of the mesoscale model and the numerical experiments are presented in section 5. The results and the applicability of the DA to real time forecast are discussed in section 6. The conclusions are given in section 7.

2 Meteorological Situation

Only a brief description of the meteorological situation characterizing the 4-6 November 1994 Piedmont flood is presented, whereas a detailed presentation of this case can be found in Massacand et al. (1998), Buzzi et al. (1998), Ferretti et al. (2000) and several other papers. A deep low level cyclone was located over the western side of Ireland and it was associated with high pressure field over eastern Europe (Fig.2a), both of which extended to the upper levels (Fig.2b), and lasted for the whole period. At 1200 UTC 4 Nov 1994, a tongue of warm and humid air (Fig.3a) was advected northward, impinging on the Gulf of Genoa and on the western Alps; 36h later, the cold front (strong temperature variation associated to an abrupt changes of the wind direction) reached the western coast of the islands of Sardinia and Corsica (Fig.2c,d, 3b). The high pressure field was stationary over the Balkans region and it slowed down the eastward movement of the trough allowing only for a counterclockwise rotation of the axis. The infrared satellite images at 1200 UTC and 1800 UTC 5 Nov 1994 show a bright band of clouds moving south-eastward (Fig.4a,b) and decreasing its intensity; during the following 6h (Fig.4c), the band became wider and more intense.
The 24h accumulated precipitation ending at 0600 UTC 6 Nov 1994 shows (Fig.5) heavy rainfall on the western side of the Alps and over the Piedmont area, with a few stations recording more than $300mm$. The areal distribution of the heavy rainfall would infer two maxima greater than this value. Furthermore, a band of precipita-

tion extended toward the western side of the Tyrrhenian sea: a few stations over the island of Corsica recorded values higher than $200mm$ (Fig.5). The satellite image (Fig.4b) would suggest heavy precipitation also off the eastern coast of Sardinia.

3 Data Assimilation

A Data Assimilation process is used for this study, which is composed as follows: OA of surface and upper-air data, using Cressman or Multiquadric techniques, and the ECMWF analyses, that are "cycled back" into the analysis, are used together. At the end of this process a new set of I.C. and B.C. is produced, which may include more information on the local circulation than the ECMWF analyses. The meteorological variables used for OA are: wind, temperature, water vapor and surface pressure; the ECMWF analyses are used as if they were a First Guess.

3.1 Objective Analysis

OA enables the modification of the data analyses using the observations: every meteorological variable at a grid point is corrected by a function which depends on the distance between the grid point and the station. Two different schemes are used for OA: the Cressman, with both circular (CRS) and banana shape (BN), and the Multiquadric (MQD). The first one (Cressman, 1959) modifies the analyses on those grid points present inside a circular area centered at the station location, according to the equation

$$\alpha'_{i,j} = \alpha_{i,j} + \frac{\sum_{k=1}^{N} w_{(i,j),k} D_k}{\sum_{k=1}^{N} w_{(i,j),k}} \tag{1}$$

where $\alpha_{i,j}$ is the analysis at i,j point, N is the total number of the stations used by the OA. D_k is the difference between the k-th observation and the analysis at the station location, and $w_{(i,j),k}$ is the weight function given by:

$$w_{i,j} = \frac{R^2 - d_{i,j}^2}{R^2 + d_{i,j}^2} \tag{2}$$

where R is the radius of a circular area and $d_{i,j}$ the cartesian distance between the grid point and the k-th station.
BN (Benjamin and Seaman, 1985) is a particular case of CRS scheme: when OA analyses is applied to the wind and the relative humidity, if the wind is larger than a critical value v_c, which depends on the pressure level, the circular area of the standard Cressman scheme becomes deformed and it follows the streamlines.

Therefore, the distance $d_{i,j}$ is corrected by

$$d_{i,j} = \left(\frac{|r_k|^2 \left(\Theta_k - \Theta_{ij}\right)^2}{1 + \beta |v_k|} + \left(|r_k| - r_{ij}\right) \right) \tag{3}$$

where Θ_k and Θ_{ij} are the angles from the positive x-direction to the line between the center of curvature and, respectively, the k^{th} observation (Θ_k) and the grid point (Θ_{ij}). r_k is the radius of curvature of the streamline at the k^{th} observation point and r_{ij} is the distance from the center of curvature to the grid point (i, j). β is the elongation of the ellipse, depending on v_c, and v_k is the wind at the station location. After this correction, the area of influence acquires a banana shape and, under low-wind conditions, BN converges to CRS. BN does not apply to the temperature field as, usually, it does not exhibit along-flow streakiness.
The MQD scheme (Nuss and Titley,1994) works on the whole domain, adjusting every grid point, according to the equation

$$\alpha'_{i,j} = \alpha_{i,j} + \mathbf{Q_{(i,j),k}} \left[\mathbf{Q_{k,m}} + \left(N \lambda \sigma_k^2 \delta_{k,m} \right) \right]^{-1} \mathbf{D_m} \tag{4}$$

where λ is a smoothing parameter, δ_{km} is the Kronecker delta and σ_k^2 is the statistic error associated to the meteorological variables. $\mathbf{Q_{k,m}}$ and $\mathbf{Q_{(i,j),k}}$ are the matrices of the radial functions depending on the distance between the k-th observation and, respectively, the other stations (m) and the grid point (i, j). The normalized radial functions depend on the multiquadric parameter c $(0 < c < 1)$ that is an index of their sharpness, as shown by the following equation:

$$Q_k(x_m, y_m) = - \left(\frac{|x_m - x_k|^2 + |y_m - y_k|^2}{c^2} + 1.0 \right)^{\frac{1}{2}} \tag{5}$$

These two techniques use a different approach: CRS (or BN) (eq.1) corrects the values at each grid point accounting only for the observations enclosed into the circular (or banana shape) area and it does not account for the errors coming from the measurements; on the other hand, MQD (eq.4) corrects the values at each grid point using the whole data set and it accounts for the statistical error in the measurements. Therefore, using MQD, a good set of I.C. and/or B.C. could be obtained over those areas with no observed data, as for the sea side.
To verify this capability, several tests using both MQD and CRS, are carried out to generate the new set of I.C. and B.C.. The sensitivity of the two schemes to both the number of the stations and their spatial distribution is investigated.
As reference, the ECMWF data analyses are used as I.C. and B.C. without applying DA (A-CNTR, test 1, table 1).
DA is performed by using together the observations available over Europe (surface pressure and upper air data) and the ECMWF data analyses; figure 6 shows both surface pressure (dot points) and upper air recording stations (the other symbols).

The first DA test (test 2) is carried out using the whole set of surface pressure available data (they are used for all DA tests) and nine radiosoundings (the circles in Fig.6); this set of data represents the minimum number of stations containing the main meteorological characteristics of the Piedmont case to produce a good new set of I.C. and B.C.. Sensitivity tests to the station location are performed adding stations far away from the flood area: the stations indicated by the asterisks in Fig.6 are added for test 3; the cross and the plus symbols for tests 4 and 5, respectively. All the DA tests (table 1), are performed using the same parameters for each scheme: the radius of influence is $R = 12.8$ for CRS, the multiquadric and smoothing parameters are, respectively, $c = 0.01$ and $\lambda = 0.0025$ for MQD. The DA is applied to the coarse domain only for all the tests, because there are not enough available radiosoundings in the inner domain.

4 Initial conditions

First of all, a comparison is performed between the new mesoscale I.C. (results of the DA tests from 2 to 5 in table 1) and both the observations and the I.C. produced without DA (A-CNTR, i.e. the ECMWF analyses interpolated to the model grid). The comparison is carried out for the Sea Level Pressure (SLP), the water vapor (q_v) and the temperature (T). The 1000hPa level is chosen for the q_v and T produced by DA, because of the differences existing between the stations elevation and the model first level. Therefore discrepancies are expected between the observations and the meteorological parameters produced by DA.
The Sea Level Pressure (SLP) does not show sensitivity to the number of the radiosoundings used for DA, for both schemes because of the large number of the surface pressure data. Therefore, only one case for CRS and MQD is shown. SLP shows, a good agreement with the observations (Fig.7), for both schemes; indeed the local high pressure on the northeast of the Po Valley (Fig.1) is better reproduced by CRS (Fig.11a) and MQD (Fig.11b) than by A-CNTR (Fig.10a). Furthermore, MQD correctly reproduce a spatial oscillation of the surface pressure in the south-west of Italy, whereas both CRS and A-CNTR miss this feature.
A few test were performed to tune the λ and c parameters for MQD; a large sensitivity to these parameters was found for SPL at the Initial Conditions, but no comparable variation was found in the model results. The precipitation forecasts produced using either the different λ or c parameters were similar to CNTR, therefore they will not be furtherly discussed.
A different response to DA is obtained for the water vapor content, because some sensitivity is found to the assimilation of the upper air data. Differences in the water vapor content between CNTR (Fig.10b) and the experiment performed using 14 radiosoundings (Fig.12a) are found over the sea, between the islands of Majorca and Sardinia, and over Tyrrhenian sea. Furthermore, there is a considerable reduction of the water vapor content over the north-west of Italy. A rather strong

reduction of the 13 g/kg contour over the western Mediterranean sea is obtained adding the radiosounding of Majorca for CRS (Fig.12b). This suggests a strong dependence on the station location for CRS scheme. A further assimilation of a few radiosoundings (up to 34 stations) located in northern Europe and in central and southern Italy, produces a widening of the 8 g/Kg contour over the Mediterranean region only (Fig.12c). This indicates that the assimilation of the stations located far from the flood area does not have any influence on the q_v distribution. The BN (Fig.12d), shows a small increase of the 13 g/kg contour over the western Mediterranean sea, using 14 radiosoundings only; furthermore, the tongue of humid air penetrates deeper, between the island of Sardinia and the western coast of Italy. BN has the effect of increasing the water vapor surface gradient over the western Mediterranean sea, that was a key factor for the flood (Rotunno and Ferretti, 2001). Generally, data analysis shows difficulties in reproducing the pattern of the q_v content over the western Mediterranean sea, because of the lack of observations over this area. Furthermore the 8.0 g/kg contour shrinks, in the central region of Italy, producing stronger horizontal gradients also over this area, but, unfortunately, there are no observations to compare, on the center-south of Italy. On the whole, BN shows a better agreement with the observations than the others, except for A-CNTR over the Po Valley (Fig.8).
Also the lack of observations over the sea does not allow verification of the distribution pattern; however, DA results show a good agreement with observed data over land, especially along the coasts, for all cases. A discrepancy between DA and the observations over the other areas may be related to the mountains.
Also MQD shows sensitivity to the stations location, the assimilation of 14 radiosoundings shows changes over the western Mediterranean sea only (Fig.13a) with respect to A-CNTR (Fig.10b). The assimilation of the radiosounding of Majorca produces a reduction of the water vapor content over the western and southern Mediterranean sea (Fig.13b). When radiosoundings over central Italy (34 stations) are used, we observe an increase of the area inside the 8 g/kg contour (Fig.13c) and a further reduction of the area inside the 12 g/kg contour, over south-western Mediterranean sea . However, also in this case, there are no observations to compare with.
The temperature field over the sea shows sensitivity to the number and the distribution of the radiosoundings for the CRS scheme. The experiment performed using 14 radiosoundings shows an increase of the temperature over the islands of Sardinia and Corsica and along the west coast of central Italy (Fig.14a) with respect to A-CNTR (Fig.10c). A further increase of the total number of the radiosoundings, from 25 up to 34, does not show any change, therefore, only the 34 stations experiment is presented. The assimilation of the Italian radiosoundings (34 stations experiment) causes a change of the 21 $^{\circ}C$ contour located over these areas (Fig.14b), producing a minimum of the temperature in the southern part of Italy. Nevertheless, the temperature pattern shows a good agreement with the observations (Fig.9).
MQD shows a small sensitivity to the 14 assimilated radiosoundings producing

changes in the temperature pattern (Fig.10c and 15a) mostly along the Italian coast (on the Tyrrhenian sea). Similarly to CRS, the increase of the stations from 25 to 34 does not produce any change, therefore only the 34 stations experiment is presented. If the stations on the south Mediterranean sea are used (Fig.15b), a temperature reduction is obtained along the Italian western coast. On the whole, both CRS and MQD show a good agreement with the observations. The previous analyses suggest that both schemes can be used to produce initial conditions, but the number and the location of the stations have to be carefully chosen, especially if CRS is used. MQD does not show strong sensitivity to the station locations except for those close to the Mediterranean area. Besides, the 34 stations experiment does not show any important difference from the others in the north Europe, which implies that the stations located in that area do not influence the initial fields.

5 Model Characteristics

The weather forecast experiments are performed using the MM5, a Limited Area Model (LAM) from PSU/NCAR (Dudhia, 1993). This is a primitive equations, fully compressible model with a terrain following vertical coordinate (σ); several parameterization for the convective precipitation and the boundary layer are available. The configuration used for this study is the one operationally used at the Science and Technology Park of Abruzzo/University of L'Aquila (PSTdA/UNIAQ) (Paolucci et al, 1999). The Kain-Fritsch (1993) cumulus convective parameterization associated with an explicit computation of rain and cloud water and the Troen and Mahrt (1986) boundary layer parameterizations are used. The model set up for this experiment uses 23 vertical levels unequally spaced, and 3 domains two way nested. The grid size is 30km for the coarse domain (51×61), 10km for domain 2 (46×55) and 3.33km for domain 3 (91×67) (Fig.1); the innermost domain is used only for the last three experiments (table 2).
A few numerical experiments are performed, using the I.C. produced by the DA tests on table 1, to study the sensitivity of the precipitation forecast to the number and the location of the radiosoundings ingested by OA. B.C. are updated every 6h using DA, if required. The experiments WF1-WF7 (see table 2) are performed using two domains and WF8-WF10 using three domains. The experiments WF7 and WF10 are performed to test the applicability of DA to the real-time forecast at low (WF7) and high (WF10) resolution. For these cases, DA is not applied to the B.C.. A simulation using 2 two-way nested domains and the I.C. and B.C., produced without DA (WF1-CNTR), is used as reference. The experiments WF2 to WF6 and WF9 are performed keeping the time step, in assimilating data, fixed at 6h and using the I.C. and B.C. improved by ingesting a different number of stations. 14 radiosoundings are used for experiment WF2, 25 and 34 radiosoundings for experiments WF3 and WF4 respectively. All the experiments show that there is not a good agreement between observed precipitation and the forecasted rainfall over the island of Cor-

sica, therefore WF5 is carried out neglecting the Ajaccio radiosounding, to study its influence on the forecast over the island. The I.C. and B.C. obtained using BN, by ingesting 14 radiosoundings, is the base for the WF6 experiment. Finally, to test the impact of DA on the real time-forecast and its applicability at the resolution of 10 km (domain 2), the WF7 experiment is carried out; the assimilation is performed using 25 radiosounding at the initial time only. A new control simulation (WF8), using 3 domains (Fig.1), is performed without using DA: this is the new reference for the last two experiments (WF9-WF10). WF9 is performed using DA for the I.C. and B.C., by ingesting 14 radiosoundings; WF10 is similar to WF7, but at higher resolution. The simulations are shown in table 2. They all start at 1200 UTC 4 Nov 1994 and end after 48h, at 1200 UTC 6 November 1994.

6 Results

The purpose of this study is to determine whether DA may improve the meso and high resolution forecast of the rainfall. Therefore, in the following paragraphs only the results for the precipitation are discussed. A comparison between the 24h accumulated precipitation produced by CNTR and the observations is carried out: the 24h accumulation period ends at 0600 UTC 6 Nov 1994, in agreement with the observations (Fig.5). Moreover, the differences between the 24h accumulated precipitation produced by CNTR and the other experiments are analyzed. The sensitivity of the precipitation forecast to a few parameters of OA and to the number of the stations at low and high resolution, and an application to the real-time forecast will be discussed.

6.1 Sensitivity to the OA parameter

Sensitivity is assessed to the variation of a few OA parameter. They are: R for CRS, λ and c for MQD. The forecast experiments performed using I.C. and B.C. obtained by reducing the radius of influence for CRS, show the convergence of the MM5 results (not shown) toward CNTR (Fig.16a), as expected.
At low resolution, if the banana shape (WF6) is used with $R = 12.8$, no significant differences are found on the areal extent and the amount of the precipitation over the Mediterranean sea, while an increase of the rainfall, west of the flood area, is observed (Fig.16c). At high resolution, the maximum over the Piedmont region is better reproduced by WF6 than by CNTR (Fig.16b), but its location is displaced. WF6 shows only a small increase of the rainfall over the flood area (Fig.16d). The differences between WF6 and CTRL are smaller than expected by the previous analyses of the I.C. produced by BN.
On the other hand, a large reduction of either the MQD parameters c (from 10^{-2} to $5 \cdot 10^{-5}$), or the smoothing parameter λ (from 10 to 10^{-6}), does not affect the forecast even if the corresponding I.C. shows improvements with respect to CNTR.

Therefore, these preliminary tests suggest that the radius of influence is the only parameter affecting the forecast of the heavy precipitation. The values of R, c, and λ, used for the evaluation of the rainfall forecast, are the ones choosen for the DA tests (par. 3.1).

6.2 Sensitivity to the number of the stations

In the following sections, sensitivity tests to the number of the upper-air stations used by OA for CRS and MQD will be presented at both low and high resolutions.

6.2.1 Low-resolution: domain 1

The observations (OBS) show (Fig.5) a wide area of light precipitation (up to $25mm$, yellow color) mostly over France (the data were not available over western France) which is reproduced by most of the model simulations. To make the figures readable, the light rainfall is not shown on the precipitation forecast. OBS shows an elongated area with a large amount of precipitation (greater than $25mm$, green and blue color on Fig.5) on the south-eastern France (close to the western Alps), and heavy rainfall is also observed in the north-western Italy (east side of the western Alps). CNTR shows a wide area of moderate rainfall over the south-eastern France (Fig.16a) in good agreement with OBS, but two bands of large rainfall are produced on this area whereas only one was observed. Moreover, the area of maximum rainfall is well localized, but it is underestimated. CNTR produces two bands of light precipitation also over the sea, which are supported by the satellite images (Fig.4a,c), as well as by previous studies (Boni et al., 1996 and Ferretti et al., 2000). The results of CNTR-WF2(CRS) experiments, performed using the I.C. and B.C. improved through the assimilation of 14 radiosoundings, show (Fig.17a) an increase of both the maxima and the areal distribution of the precipitation on the flood area. However, the rainfall remains underestimated on domain 1. An increase of the precipitation is also found over the Mediterranean sea, west and east of the islands of Corsica and Sardinia. Furthermore, CNTR-WF2(CRS) shows a reduction of the precipitation on the south-south-east of France and over the islands of Corsica and Sardinia. On the other hand, CNTR-WF2(MQD) produces a reduction of the precipitation over the flood area (Fig.17b), whereas an increase is found in the south-eastern France close to the Italian border. A decrease of the rainfall is also found on a wide area over the Tyrrhenian sea. Also in this case, the maximum of the precipitation does not match the observed value and it is even smaller than CRS.
WF3-CRS is performed adding the radiosoundings indicated by a plus sign on figure 6, which are far from the Piedmont region. Similarly to the previous case, an increase of the rainfall on the flood area and on the elongated area toward the sea is found (CNTR-WF3(CRS), Fig.17c), associated to a strong reduction of the precipitation in the south-south-east of France (CNTR-WF3(CRS), Fig.17c). Moreover, the rainfall over the two islands is not changed with respect to CNTR (Fig.16a),

showing a tendency to reduce the correction over those areas. Actually, both the maxima and the distribution of the precipitation are worse when compared with the previous case (WF2-CRS). CNTR-WF3(MQD) shows (Fig.17d) a large area of reduced precipitation over the Piedmont region and over the two islands, while at the same time an increase of the rainfall is found on a large area on the western Mediterranean sea and east of the two islands. In contrast to CNTR-WF3(CRS), an increase of the tendency to correct the rainfall around the islands is found for CNTR-WF3(MQD).
Finally, WF4-CRS and WF4-MQD both confirm the tendency previously found. Over the sea side (Fig.17e), the difference between CNTR and WF4(CRS) is reduced, and this results in an improvement of the precipitation forecast. On the other hand, the comparision CNTR-WF4(MQD) shows a strong reduction of the rainfall over a wide area enclosing the Piedmont region, and a large increase of the precipitation over both the south-eastern France and the elongated area toward the sea (Fig.17f). For both these two last experiments, radiosoundings located on the northern Europe, on the south-central Italy and on the Mediterranean area are added.
In summary, as the number of radiosoundings ingested by OA increase, a reduction (or no correction) of the rainfall over the Tyrrhenian sea for CRS is found. For MQD, a strong reduction over the central Mediterranean sea and a large increase in the western side are found. These results suggest a strong sensitivity to the number of radiosoundings used by OA, over the area where no observations are available.

6.2.2 High-resolution: domain 2

Generally, at high resolution a good agreement between CNTR (Fig.16b) and OBS (Fig.5) is found, although the model underestimates the precipitation over the area of the flood and also in the eastern side of the Maritime Alps, where another maximum is observed.
WF2-CRS shows a good skill in reproducing the precipitation at this resolution: the maximum over the flood area (not shown) is very close to the observations. CNTR-WF2(CRS) shows an increase of the rainfall over this area only (Fig.18a). On the other hand, CNTR-WF2(MQD) does not produce an improvement of the forecast, also at this resolution (Fig.18b). In this case, a slight decrease in the maximum of the precipitation is obtained. Similarly to the low-resolution cases, a further increase in the number of the radiosoundings (far away from the Piedmont region) produces a considerable change in the precipitation forecast, but it is negative especially for MQD. CNTR-WF3(MQD) produces a more severe underestimation of the precipitation (Fig.18d) than the previous case, whereas small differences are found between CNTR-WF2(CRS) and CNTR-WF3(CRS) (Fig.18c). In this case, the increased precipitation moves slightly northward.
The assimilation of 34 radiosoundings (WF4-CRS) produces two maxima of heavy precipitation on the flood area (not shown) and a reduction of the minimum on the

lee side of the Maritime Alps (CNTR-WF4(CRS), Fig.18e), both in good agreement with OBS. On the other hand, CNTR-WF4(MQD) reduces the rainfall both on the flood area and south of it, therefore, the underestimation of the maximum over the flood area still persists (Fig.18f).
In summary, CRS shows a weak sensitivity to the number of the radiosoundings used for DA, whereas both the CRS and MQD schemes show sensitivity to the location of several stations. Furthermore, the precipitation forecast is not a linear function of the number of the radiosoundings used for DA, indeed the assimilation of the stations far away from the target area (Piedmont), may produce negative effects, for both high and low resolution. It is noteworthy that the Data Assimilation produces a gain into the precipitation forecast at low and high resolution if 14 stations (WF2) or if stations in the upwind side are used, as for WF4. The sensitivity to a single station, WF5 experiment, did not show any improvement of the precipitation near the island of Corsica (not shown).

6.2.3 Highest resolution: domain 3

A large amount of rainfall was observed at three stations in the flood area, recording values greater than $300mm$. Two of these stations are not distinguishable in OBS, therefore only two maxima are assumed. Finally, the two maxima are obtained increasing the resolution only (WF8, the new CNTR) (Fig.19a): a second maximum is resolved in the northern part of Piedmont, reaching $277mm$, associated to a reduction of the minimum south of the flood area. But the maxima are underestimated. The feedback on the lower resolution allows to resolve the two maxima on domain 2 also, but on domain 1 only one maximum is obtained (not shown), and the underestimation is still large. CNTR-WF9(CRS) (Fig.19b) shows an increase of the precipitation on the northern side of Piedmont and a slight decrease of the rainfall over the region of the second maximum. Two maxima are produced (not shown) reaching approximately the right amount of precipitation: $318mm$ and $303mm$, compared to the observed values in the same area at $351mm$ and $304mm$. In this case the feedback at lower resolution begins to resolve the second maximum also on domain 1, allowing for a good estimation of the rainfall (not shown). On the other hand, CNTR-WF9(MQD) (Fig.19c) does not show a sensible increase of the rainfall. Also in this case two maxima are obtained, but they are both underestimated (Fig.5), as it is found at low resolution (not shown). It is well known that, as the resolution increases, an increase in the rainfall is obtained, as shown by the CNTR experiment (Fig.19a). However, in this case a further improvement is obtained with DA. The amount of precipitation and the location of the maxima are both very well reproduced by CRS. This would suggest that this scheme is a good tool at high resolution.

6.3 The DA and the real-time forecast

A few experiments, using both CRS and MQD, are performed to test the applicability of DA to the real-time forecast at both high and low resolution. To meet the requirement and be a real-time forecast, DA is applied to the I.C. only. A few similarities are found between CNTR-WF7 (Fig.20a,b) and the experiment performed applying DA to both I.C. and B.C. (WF3, Fig.18c,d) at the same resolution (10km), but a better agreement with OBS is found for both WF7-MQD and WF7-CRS than for WF3. A small increase of the rainfall over the flood area is produced by both experiments, but the maximum is better reproduced by CRS than MQD. Furthermore, the splitting of the maximum over the flood area is obtained using CRS, as for WF4. The feedback alse contributes to the improvement of the precipitation forecast at low resolution (not shown). These results would suggest that DA may be successfully applied to the real-time forecast at this resolution. If higher resolution is used (WF10, 3.3km) the splitting of the two maxima is found for both CNTR-WF10(CRS) (Fig.21a) and CNTR-WF10(MQD) (Fig.21b), but still the maxima are underestimated. Only a small impact on the precipitation forecast is found, in this case. At lower resolution, on both domain 1 and 2 and for both schemes, the feedback allows to resolve the two maxima, but MQD still underestimates both of them (not shown). These results suggest that DA may improve the rainfall for this case at a resolution of 10km, whereas at higher resolution only small corrections are produced.

7 Conclusions

The Data Assimilation of the observations is used with the purpose of improving precipitation forecast. A well known heavy precipitation event, the 4-6 November 1994 Piedmont flood, is used as test case.
The purpose was to build the best mesoscale I.C. and B.C., containing as much information as possible over the whole area, expecially where the data are scarce. Despite the fair forecast for the heavy precipitation, already obtained without using DA, we are interested in improving the precipitation forecast around the flood region and also far from that area, as for example over the island of Corsica, where the model clearly underestimated the rainfall.
To improve the mesoscale I.C. and B.C. two different schemes, Cressman and Multiquadric, are used for OA. Preliminary tests and tuning of the two schemes show sensitivity to a few parameters suggesting that special care has to be taken for the radius of influence using CRS: the choice of this parameter depends on the grid size of the model domain. MQD shows sensitivity either to the multiquadric and to the smoothing parameters in generating the I.C. and B.C., but the impact on the precipitation forecast is negligible.
The comparison between the mesoscale I.C., computed using DA, and the observations suggests that DA is a simple method to improve the ECMWF data analyses.

A considerable impact on the water vapor content and on the surface temperature is found over flat areas; both q_v and T produced by DA, show a better agreement with the observations than the ECMWF data analyses, which are normally used for the weather forecast. The assimilation performed ingesting a different number of radiosoundings shows sensitivity to the location of most of the stations for CRS, whereas MQD shows sensitivity to the stations close to the Mediterranean area only. The assimilation of stations far away from the area of interest may produce a negative impact on the precipitation forecast as WF3 experiment shows. CRS shows a small sensitivity to the station location; if the stations close to Mediterranean area are used, CRS shows a tendency to produce no changes especially over the sea. MQD shows strong sensitivity and the opposite tendency, with respect to CRS, as the stations close to the Mediterranean area are used. Therefore, it may be more appropriate to use the CRS scheme over areas with sparse data.
On the whole, the entire set of experiments indicates a positive impact of the data assimilation at coarse and high resolution, whereas a few negative effects are found depending on the location of the stations used for DA. Sensitivity of the data assimilation to the resolution was showed by Stauffer and Seaman (1994), but in this case it was not possible to explore the impact on the higher resolution only, because of the lack of radiosoundings on the third domain. The data assimilation produces an improvement of the precipitation forecast at each resolution using CRS, for both real-time forecast and model simulations. On the other hand, MQD does not improve the precipitation forecast, indeed an underestimation of the rainfall is found. A considerable improvement in the simulation of the precipitation is obtained if high resolution ($3.33km$) is used, including a splitting of the maximum (WF9) of precipitation. However the simulations performed without applying DA underestimate the rainfall, whereas a total rainfall close to the observed values is obtained if DA is applied either to the forecast (WF10-CRS) or to the simulation (WF9-CRS).
Unfortunately, DA did not show any gain in the precipitation forecast over the island of Corsica, suggesting that the rainfall was produced by convection embedded into the large scale, as already stated by Boni et al. (1996). Stauffer and Seaman (1990) had similar difficulties in reproducing convective precipitation also using the FDDA (nudging). This may imply that the model has difficulties in dealing with convective precipitation over areas where the orographic uplifting is not strong. Indeed, despite the overall good skill of the MM5 in forecasting the flood, there is a clear displacement in the location of the maximum of the precipitation toward regions with steep orography. This suggests a model tendency to produce precipitation if a strong uplifting is generated either by local forcing, being the orography or local convergence areas, or by large scale forcing.
Despite the clear improvement of the I.C. shown by MQD and BN, the corresponding forecasts of the rainfall are not as good as expected. This suggests that the enhancement of the initial horizontal gradient of water vapor over the Tyrrhenian sea, that was a key factor for this case, is not enough to improve the forecast of the rainfall over the Piedmont area, as concerns these two schemes.

In summary the Data Assimilation, performed in this study, produces negative or positive impact depending on the scheme that has been used, and both on the location and amount of the stations ingested by OA. Small variations of the I.C. and B.C. may generate changes (increase or decrease) in the precipitation forecast on the flood area, whereas over the sea the changes are small and mostly produced by MQD, suggesting a strong control by the model physics on this area.

Acknowledgment
NCAR is acknowledged for the MM5 and the preprocessing software. The Science and Technology Park of Abruzzo for the computer time and the ECMWF data.

References

Bengtsson, L., 1978: Growth rate and vertical propagation of the initial error in baroclinic models. *Tellus* , **23**, 323–334

Bengtsson, L., M. Ghil and E. Källén, 1981: Dynamic Meteorology. Data assimilation methods. *Applied Mathematical Sciences 36.* 330 pp.

Benjamin, S. G. and N. Seaman, 1985: A simple scheme for objective analysis in curved flow. *Mon. Wea. Rev.*, **113**, 1184–1198

Boni, G., M. Conti, S. Dietrich, L. Lanza, F. Marzano, A. Mugnai, G.Panegrossi and F. Siccardi, 1996: Multisensor observations during the flood event of 4-6 November, 1994 over northern Italy. *Remote Sensing Reviews*, **14**, 91–117

Buzzi, A., N. Tartaglione and P. Malguzzi, 1998: Numerical simulations of the 1994 Piedmont flood: role of orography and moist processes. *Mon. Wea. Rev.*, **126**, 2369–2386

Cressman, G. P., 1959: An operational objective analysis system. *Mon. Wea. Rev.*, **87**, 367–374

Daley, R., 1991: Atmospheric Data Analysis. Cambridge Atmospheric and Space Science Series. Cambridge University Press

Dudhia, J., 1993: A nonhydrostatic version of the Penn State-NCAR amesoscale model: Validation tests and simulation of an Atlantic cyclone and cold front. *Mon. Wea. Rev.*, **121**, 1493–1513

Ferretti, R., S. Low-Nam and R. Rotunno, 2000: Numerical simulations of the Piedmont flood of 4-6 November 1994. *Tellus* , **52**, 162–180

Ghil, M. and P. Malanotte-Rizzoli, 1991: Data assimilation in meteorology and oceanography. *Adv. Geophys.*, **33**, 141–265

Kain, J. S. and J. M. Fritsch, 1993: Convective parameterization for mesoscale models: The Kain-Fritsch scheme. *The representation of cumulus convection in numerical models.* K. A. Emanuel and D. J. Raymonds, Eds., Amer. Meteor. Soc., 246 pp.

Kuo, Y.-H., Y.-R. Guo and E. Westwater, 1993: Assimilation of Precipitable Water Measurement into a Mesoscale Numerical Model. *Mon. Wea. Rev.*, **121**, 1215–1238

Lorenc, A. C., 1986: Analysis methods for numerical weather prediction. *Quart. J. R. Met. Soc.*, **112**, 1177–1194

Lorenz, E. N., 1982: Atmospheric predictability experiments with a large numerical model. *Tellus* , **34**, 505–513

Massacand, A. C., H. Wernli and H. Davies, 1998: Heavy precipitation on the Alpine southside: an upper-level precursor. *Geophys. Res. Lett.*, **25**, 1435–1438

Nuss, W. A. and D. Titley, 1994: Use of multiquadric interpolation for meteorological objective analysis. *Mon. Wea. Rev.*, **122**, 1611–1631

Paolucci, T., L. Bernardini, R. Ferretti and G. Visconti, 1999: Real-Time Forecast of a Catastrophic Event on May, 5 1998. Il Nuovo Cimento, **22**, 727–736

Rabier, F., J.-N. Thépaut and P. Courtier, 1998: Extended assimilation and forecast experiments with a four dimentional variational assimilation system. *Quart. J. R. Met. Soc.*, **124**, 1861–1887

Richard, E., J. Charney, S. Cosma, R. Benoit, S. Chamberland, A. Buzzi, L. Foschini, R. Ferretti and J. Stein, 1998: Intercomparison of simulated precipitation fields for some MAP episodes. *Map Newsletter*, **9**, 12–13

Rotunno, R. and R. Ferretti, 2001: Mechanism of Intense Alpine Rainfall. *J. Atmos. Sci.*, **58**, 1732–1749

Schraff, C. H., 1997: Mesoscale data assimilation and prediction of low stratus in the Alpine region. *Meteorol. Atmos. Phys.*, **64**, 21–50

Stauffer, D. R. and N. Seaman, 1990: Use of four-dimentional data assimilation in a limited-area mesoscale model. Part I: Experiments with synoptic-scale data. *Mon. Wea. Rev.*, **118**, 1250–1277

Stauffer, D. R. and N. Seaman, 1994: Multiscale 4-dimensional data assimilation. *J. Appl. Meteor.*, **33**, 416–434

Troen, I. and L. Mahrt, 1986: A simple model of the atmospheric boundary layer: sensitivity to surface evaporation. *Bound.-Layer Meteor.*, **37**, 129–148

	experiment	stations used
1	A-CNTR	–
2	S.C.	14
3	S.C.	25
4	S.C.	34
5	S.C.-BN	14

Table 1. Tests performed for the analysis using a different amount of stations. S.C. means standard conditions, i.e. R = 12.8 for Cressman scheme, $c = 0.01$ and $\lambda = 0.0025$ for Multiquadric. Experiment 5 is performed using the Banana shape.

	experiment	parameters	stations used	assimilation interval	correction	domains
1	WF1(CNTR)	–	–	–	I.C.-B.C.	2
2	WF2	S.C.	14	6h	I.C.-B.C.	2
3	WF3	S.C.	25	6h	I.C.-B.C.	2
4	WF4	S.C.	34	6h	I.C.-B.C.	2
5	WF5(Ajaccio)	S.C.	24	6h	I.C.-B.C.	2
6	WF6(BN)	S.C.	14	6h	I.C.-B.C.	2
7	WF7	S.C.	25	–	I.C.	2
8	WF8(CNTR)	–	–	–	I.C.-B.C.	3
9	WF9	S.C.	14	6h	I.C.-B.C.	3
10	WF10	S.C.	25	–	I.C.	3

Table 2. Numerical weather prediction experiments using different stations, performing the OA for B.C. and I.C. or I.C. only and for different nested domains. S.C. means standard conditions, i.e. R = 12.8 for Cressman scheme, $c = 0.01$ and $\lambda = 0.0025$ for Multiquadric. I.C. and B.C. are respectively initial and boundary conditions.

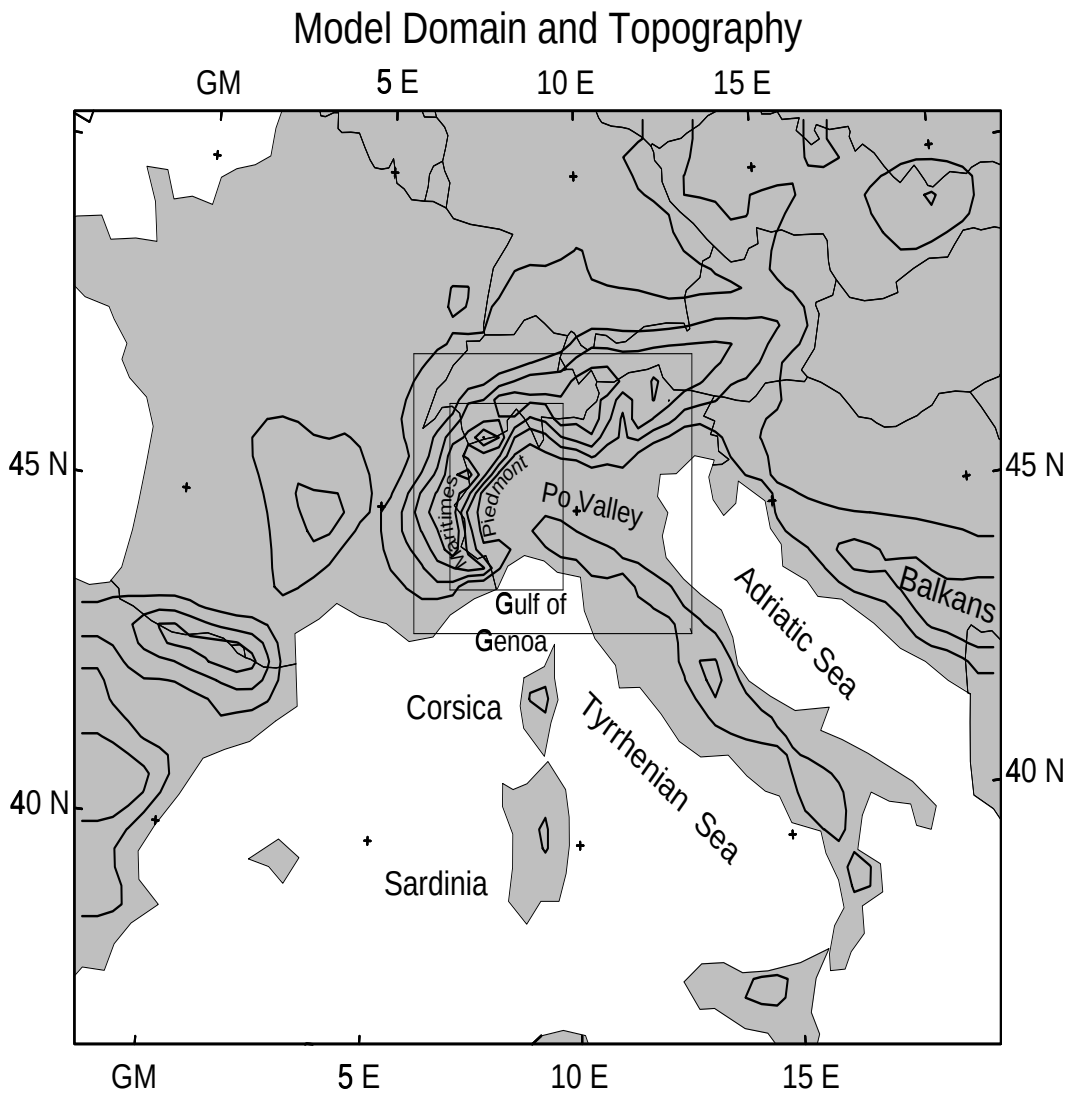

Figure 1. The model domains. The grid size are, respectively, 27km for coarse domain, 9km for domain 2 and 3.33 km for the innermost one. The third domain is centered over the Piedmont region.

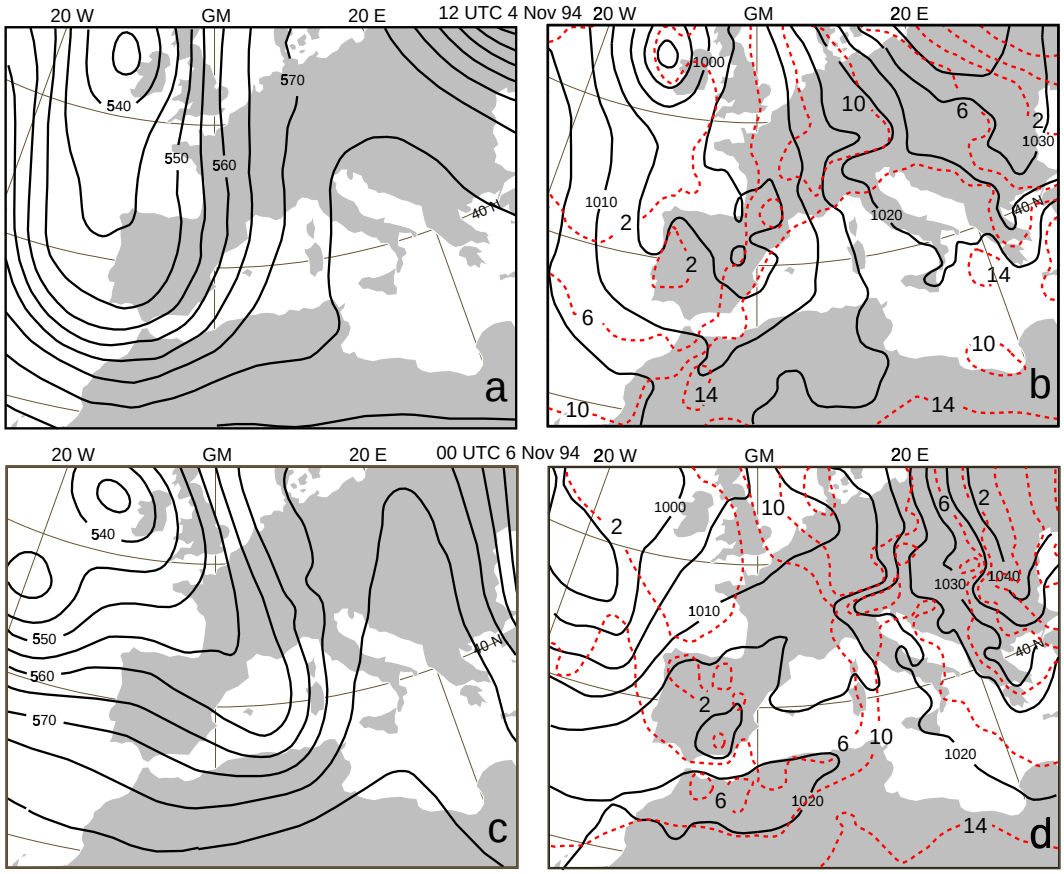

Figure 2. ECMWF data analysis of 500hPa geopotential (m), on the left panel, and surface pressure (hPa), together with 850hPa temperature ($^{\circ}C$) (dashed lines), on the right panel at 1200 UTC of 4 Nov 1994 (a,b) and 0000 UTC of 6 Nov 1994 (c,d).

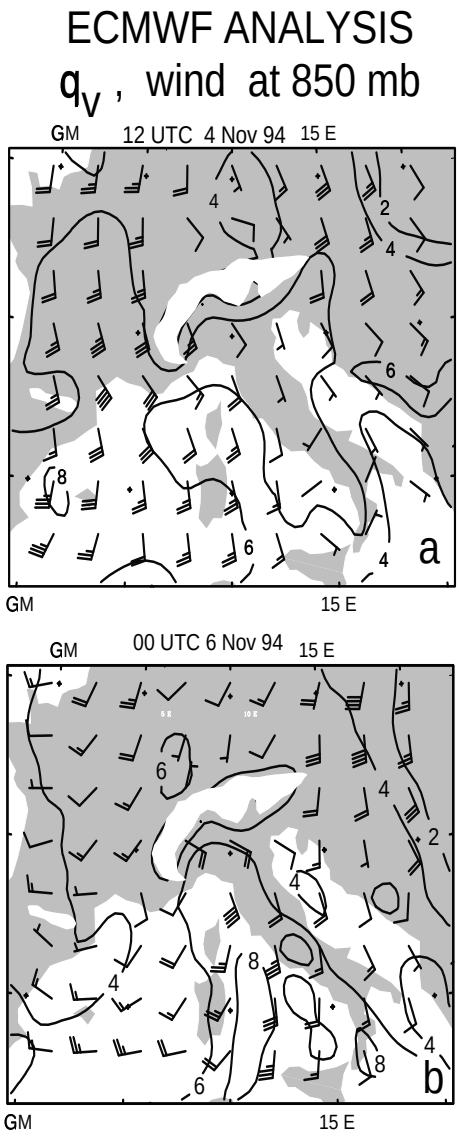

Figure 3. ECMWF data analysis of water vapor (g/Kg) at 850hPa at 1200 UTC on 4 Nov 1994 (a) and 0000 UTC of 6 Nov 1994 (b).

a) 1200 UTC 5 Nov 1994

b) 1800 UTC 5 Nov 1994

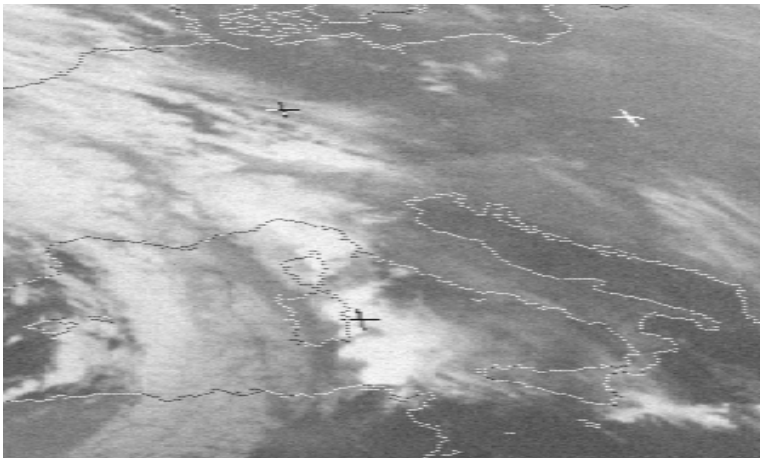

c) 0000 UTC 6 Nov 1994

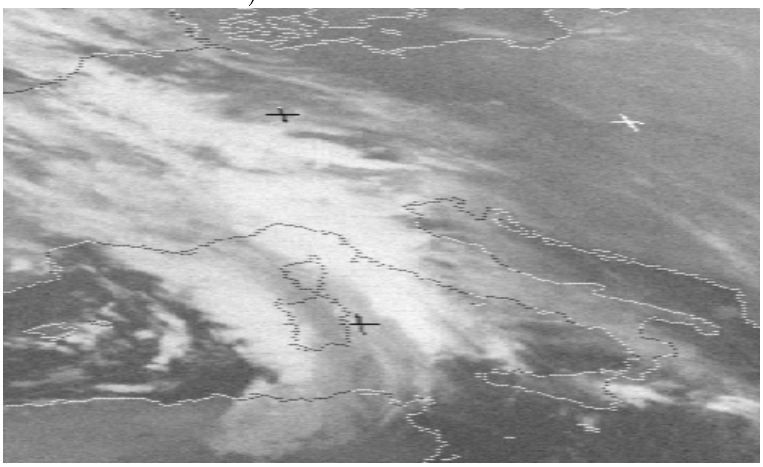

Figure 4. Infrared satellite images at: a) 1200 UTC on 5 Nov 1994, b) 1800 UTC on 5 Nov 1994 and c) 0000 UTC on 6 Nov 1994.

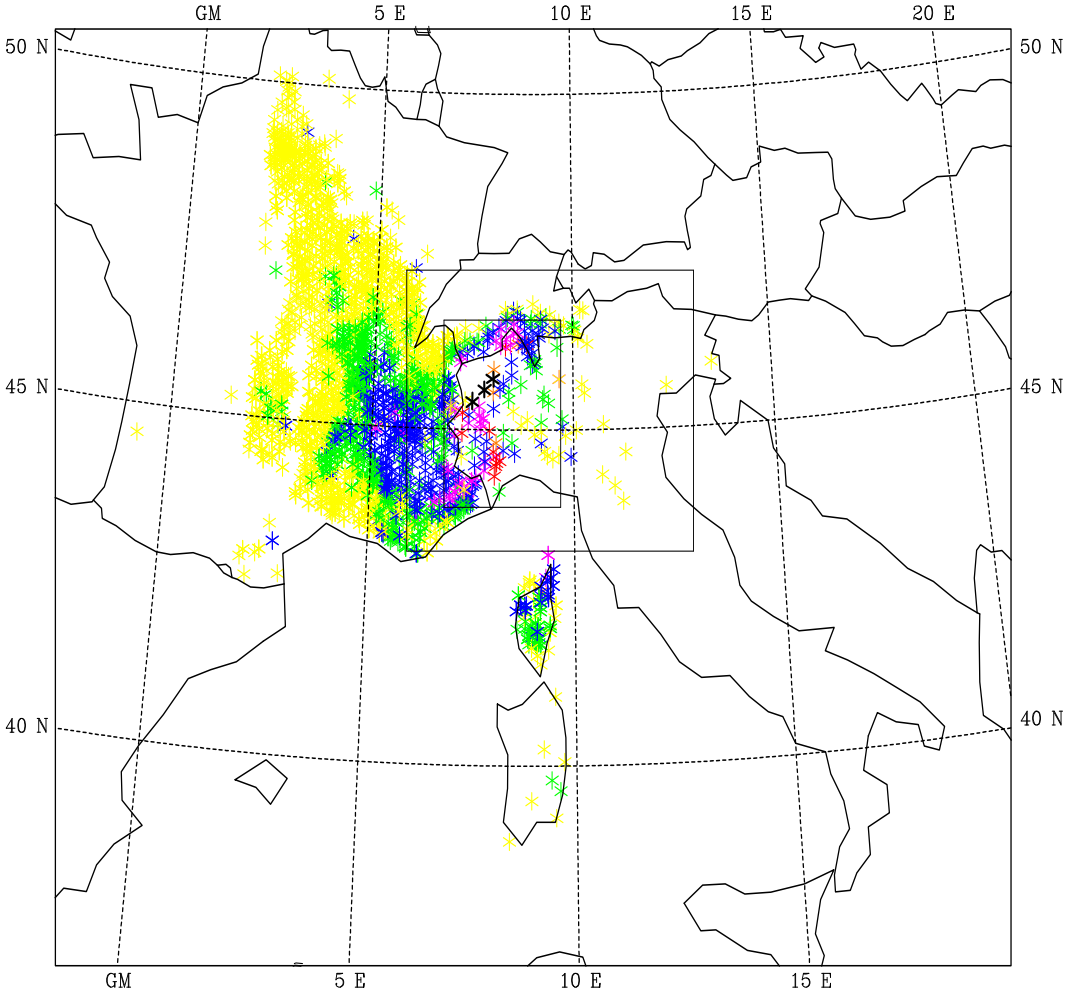

Figure 5. 24h accumulated precipitation on the coarse domain ending at 0600 UTC, 6 Nov 1994. The color code is: <25 mm yellow, 25–50 mm green, 50–100 mm blue, 100–150 mm magenta, 150–200 mm red, 200–250 mm orange, 250–300 mm sky blue, >300 mm black.

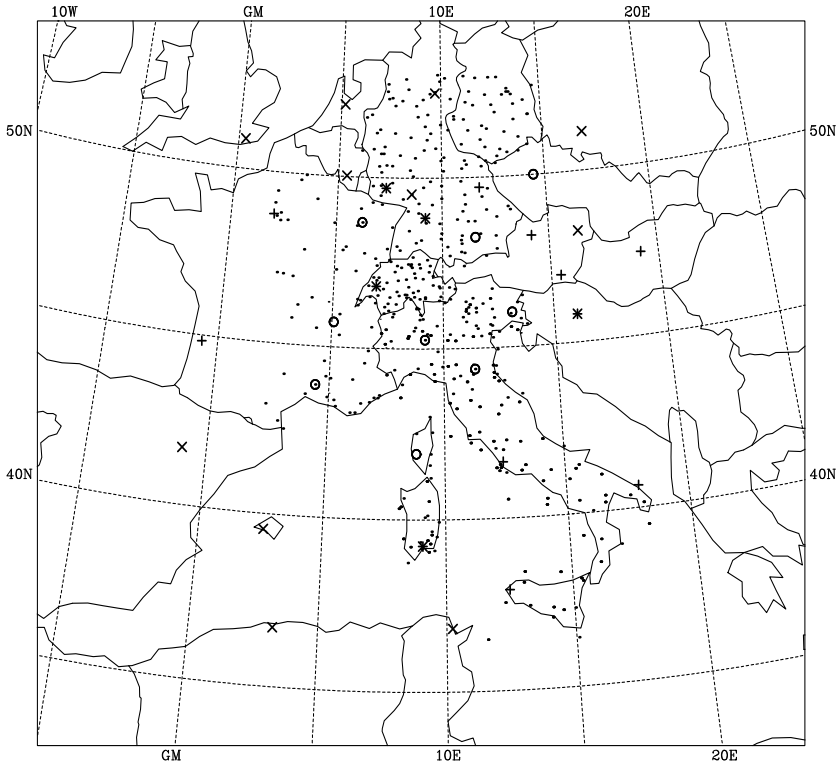

Figure 6. Observations used for the OA. The color code is: yellow-surface stations, others-upper air stations.

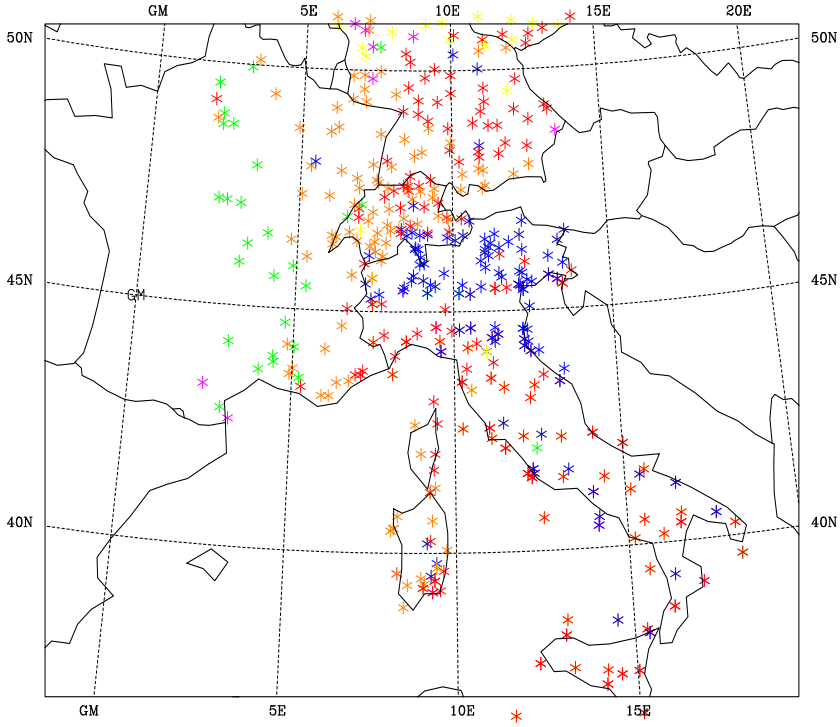

Figure 7. The observed SLP. The code color is: $\leq$ 1000 hPa yellow, 1000–1005 hPa magenta, 1005–1010 hPa green, 1010–1015 hPa orange, 1015–1020 hPa red, $>$ 1020 hPa blue.

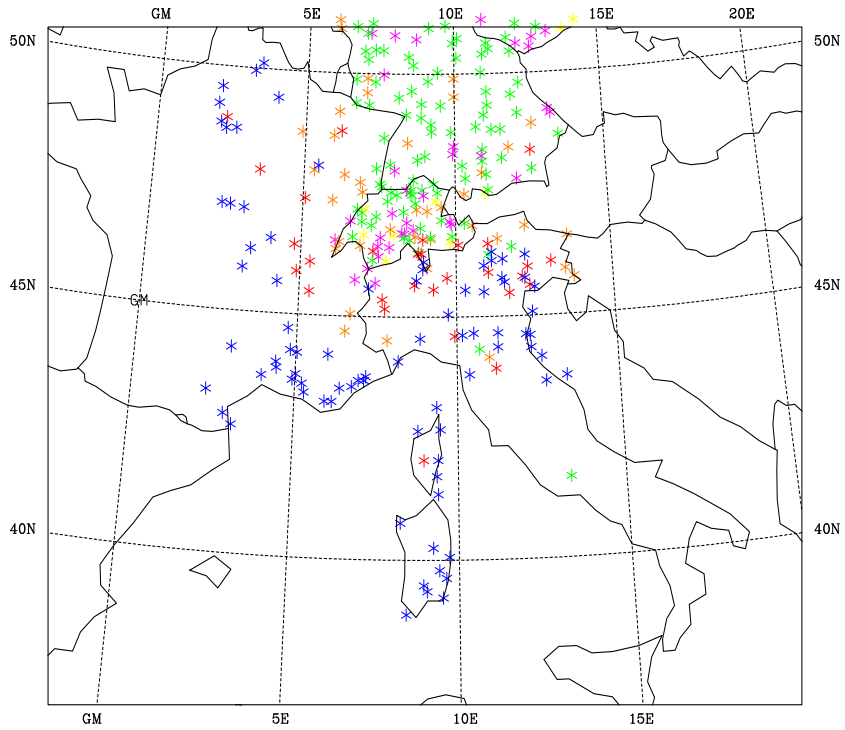

Figure 8. The observed surface water vapor. The color code is: $\leq$ 5 g/kg yellow, 6 g/kg magenta, 7 g/kg green, 8 g/kg orange, 9 g/kg red, $>$ 9 g/kg blue.

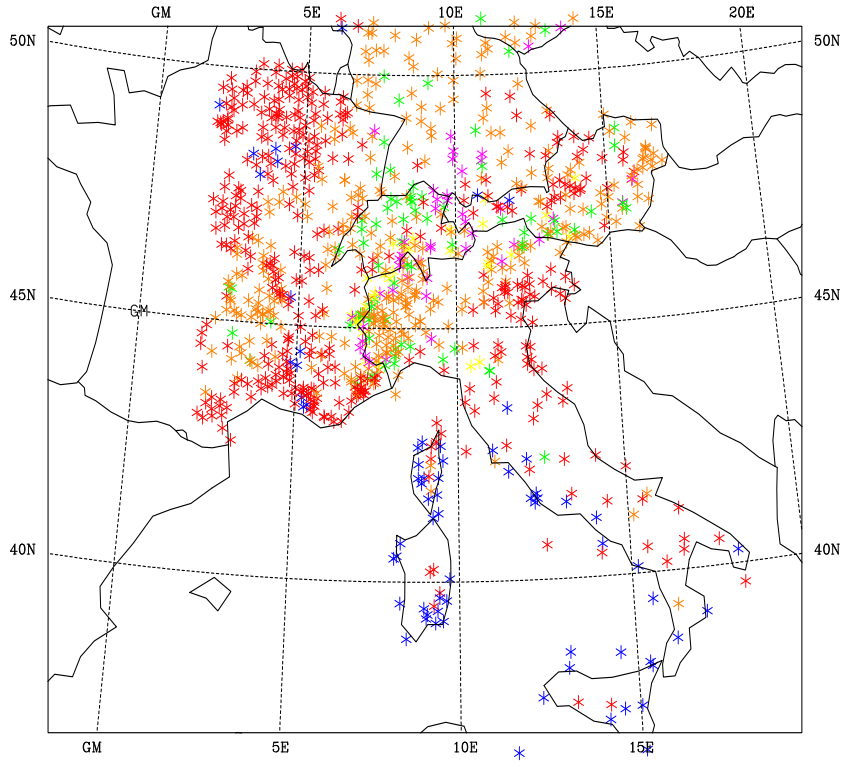

Figure 9. The observed surface temperature. The code color is: $\leq$ 5 $^{\circ}C$ yellow, 5–8 $^{\circ}C$ magenta, 8–10 $^{\circ}C$ green, 10–15 $^{\circ}C$ orange, 15–20 $^{\circ}C$ red, $>$ 20 $^{\circ}C$ blue.

a) SLP

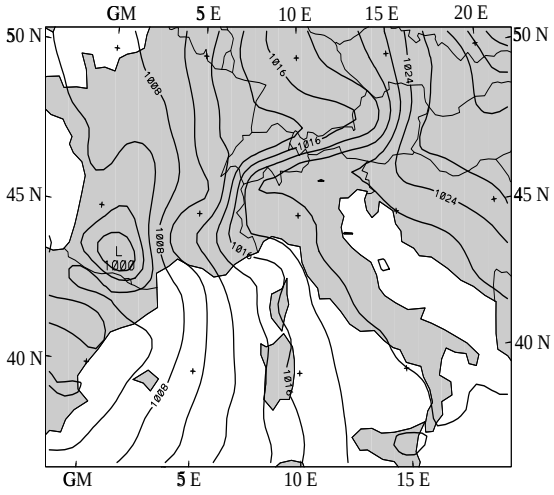

b) Q_v

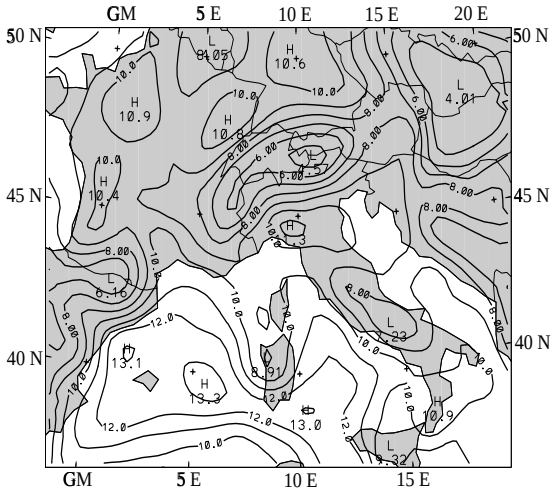

c) T

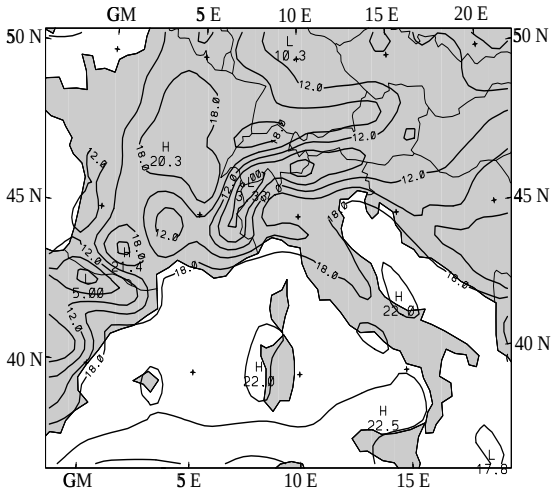

Figure 10. The analyzed a) SLP (hPa), b) Q_v (g/kg) and c) T ($^{\circ}C$) without using the OA (A-CNTR).

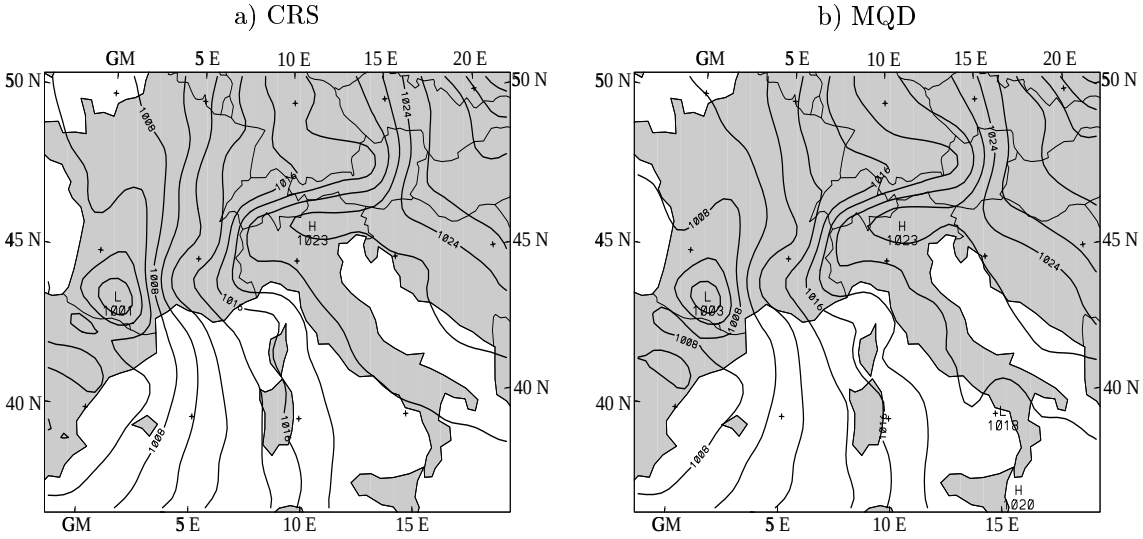

Figure 11. The analyzed SLP (hPa) for a) CRS and b) MQD.

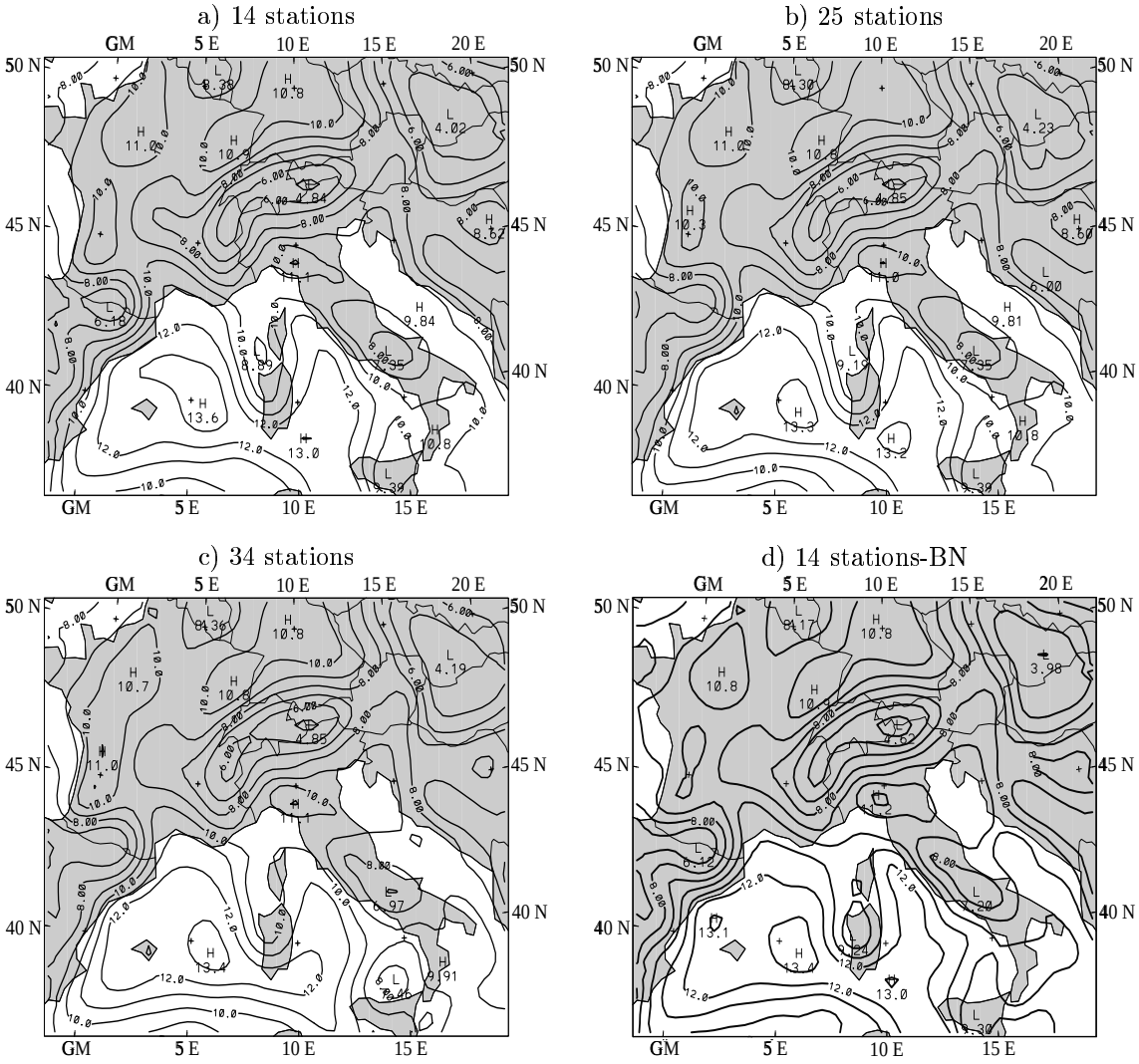

Figure 12. The $1000hPa$ water vapor analysis (g/kg) for CRS scheme using all the surface data and different number of upper air: a) 14 stations, b) 25 stations, c) 34 stations, d) 14 stations and Banana scheme.

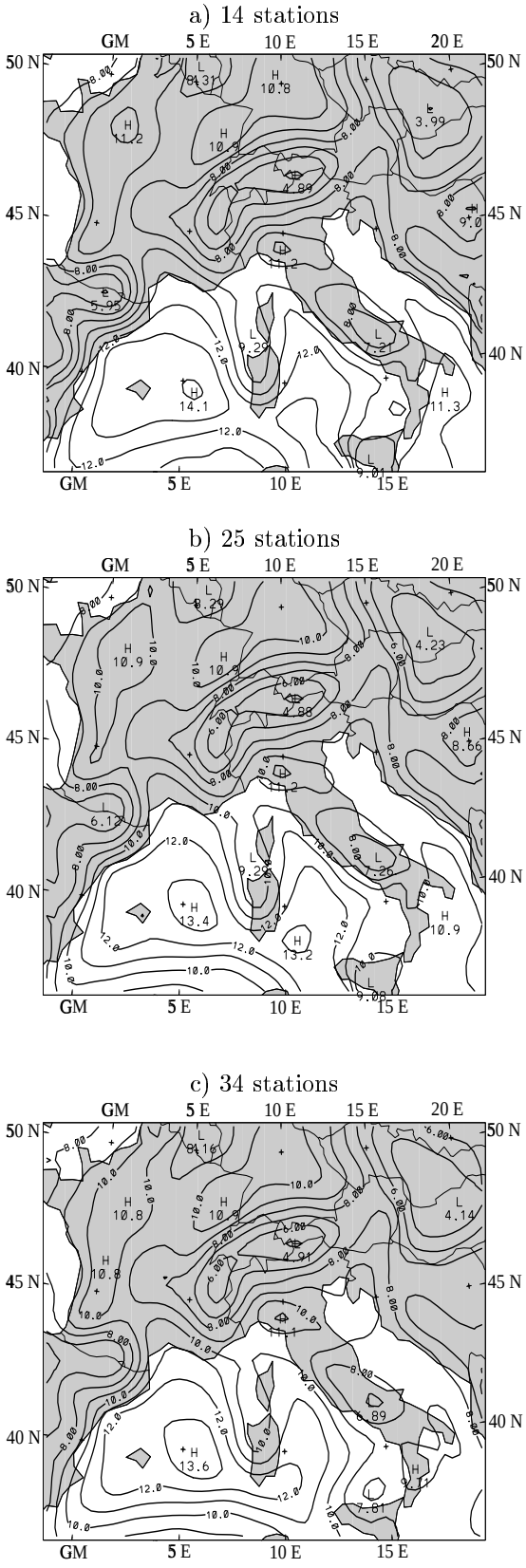

Figure 13. The $1000hPa$ water vapor analysis (g/kg) for MQD scheme using all the surface data and different number of upper air: a) 14 stations, b) 25 stations, c) 34 stations.

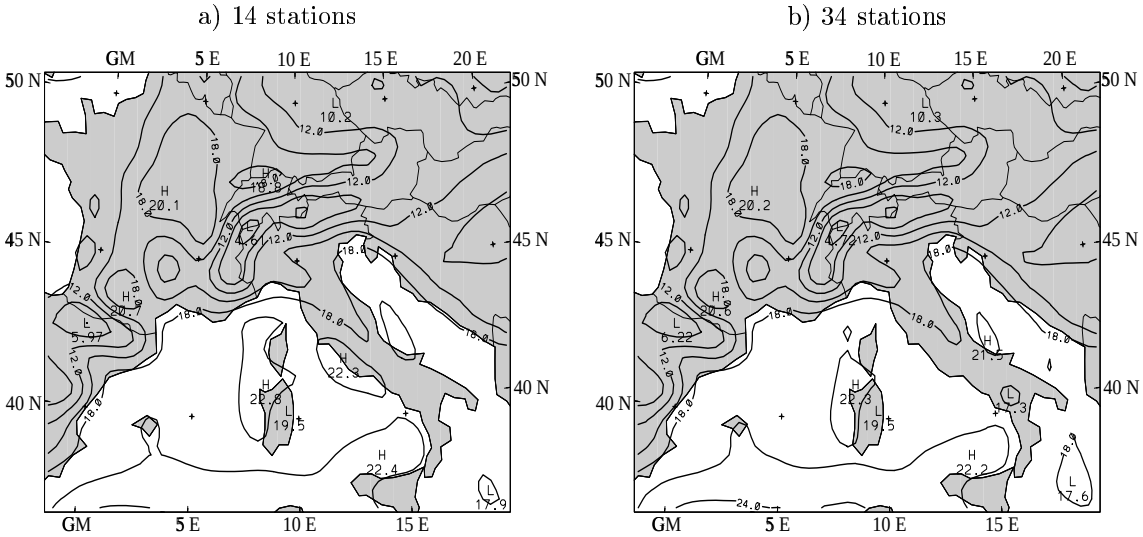

Figure 14. The $1000hPa$ surface temperature analysis ($^{\circ}C$) for CRS scheme using all the surface data and different number of upper air: a) 14 stations, b) 34 stations.

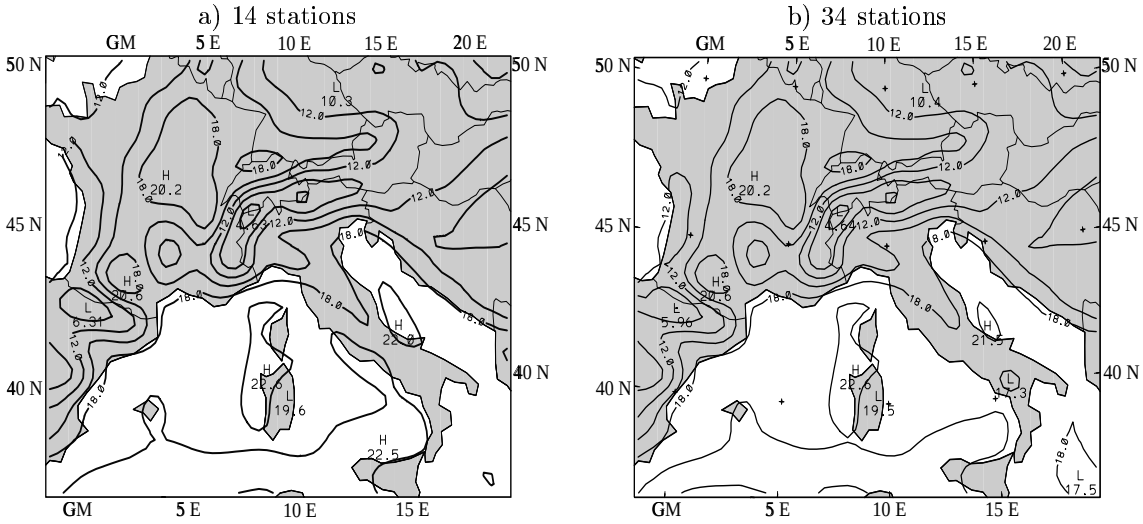

Figure 15. The $1000hPa$ surface temperature analysis ($^{\circ}C$) for MQD scheme using all the surface data and different number of upper air: a) 14 stations, b) 34 stations.

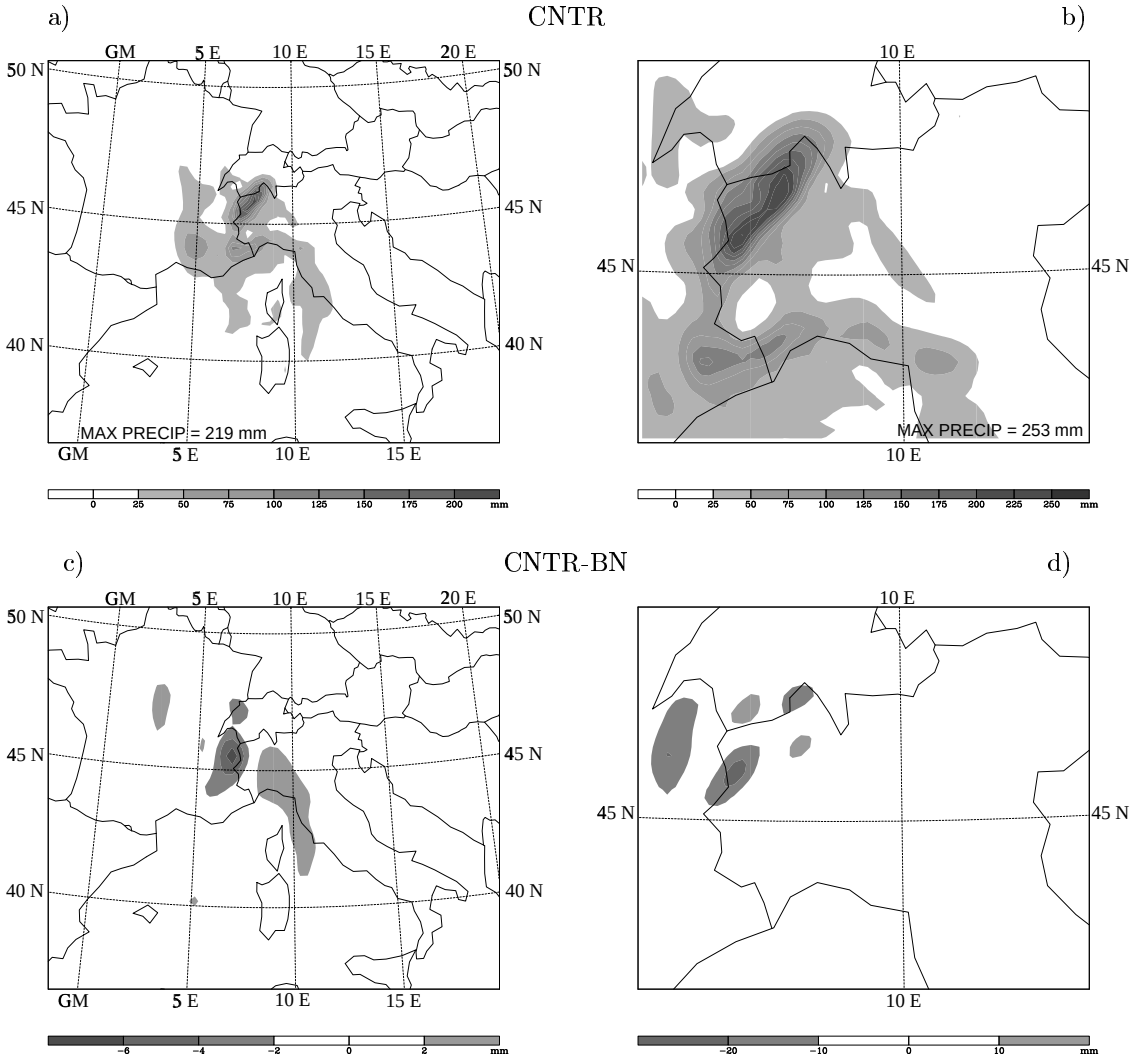

Figure 16. 24h accumulated precipitation ending at 0600 UTC 6 Nov 1994 for a) coarse and b) nested domains for CNTR. The contours interval are of 50 mm between 50 and 350 mm. Differences between CNTR and BN 24h accumulated precipitation ending at 0600 UTC 6 Nov 1994 on c) coarse and d) nested domains.

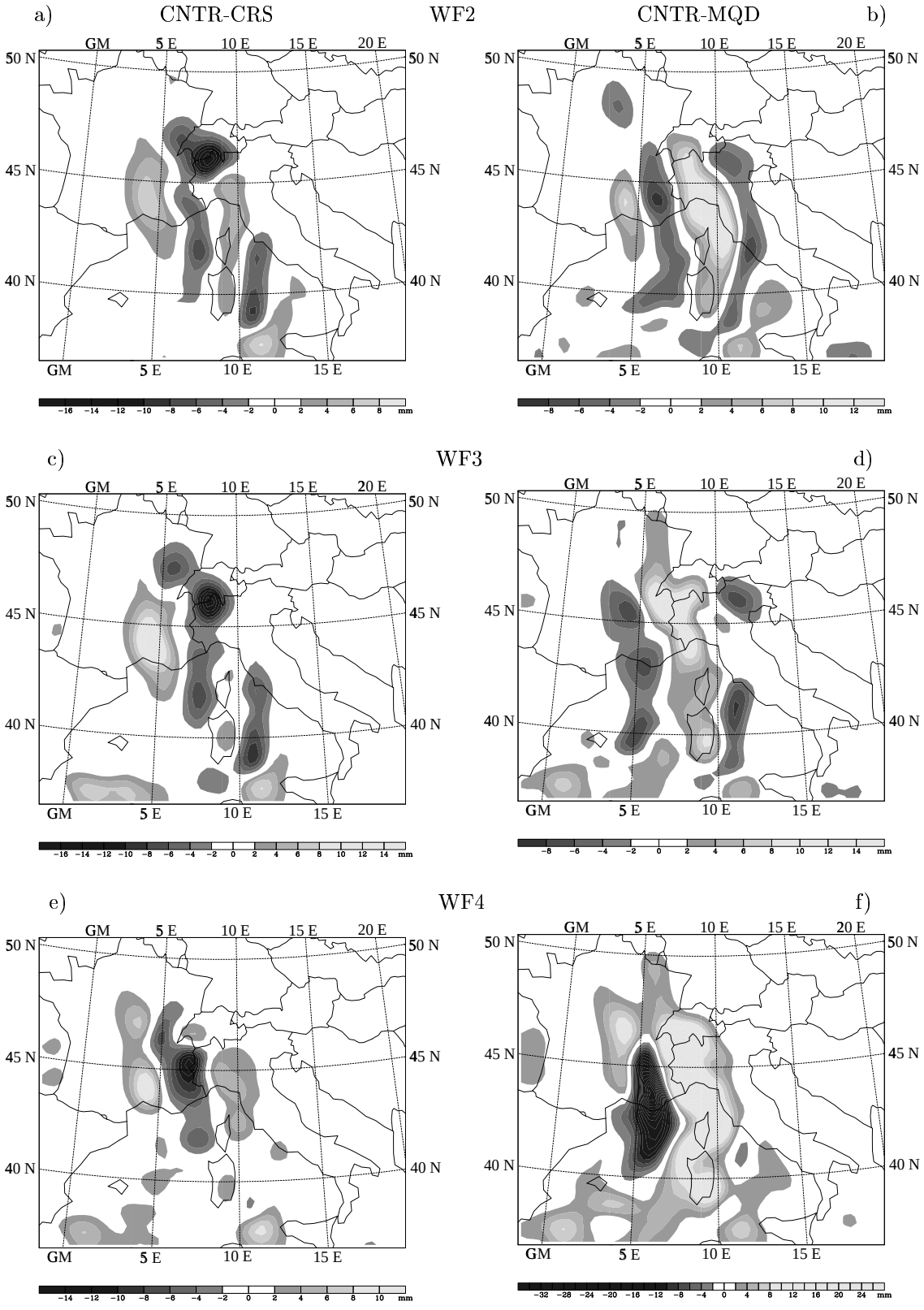

Figure 17. Differences between CNTR and a) WF2-CRS, b) WF2-MQD, c)WF3-CRS, d) WF3-MQD, e) WF4-CRS and f) WF4-MQD 24h accumulated precipitations ending at 0600 UTC 6 Nov 1994.

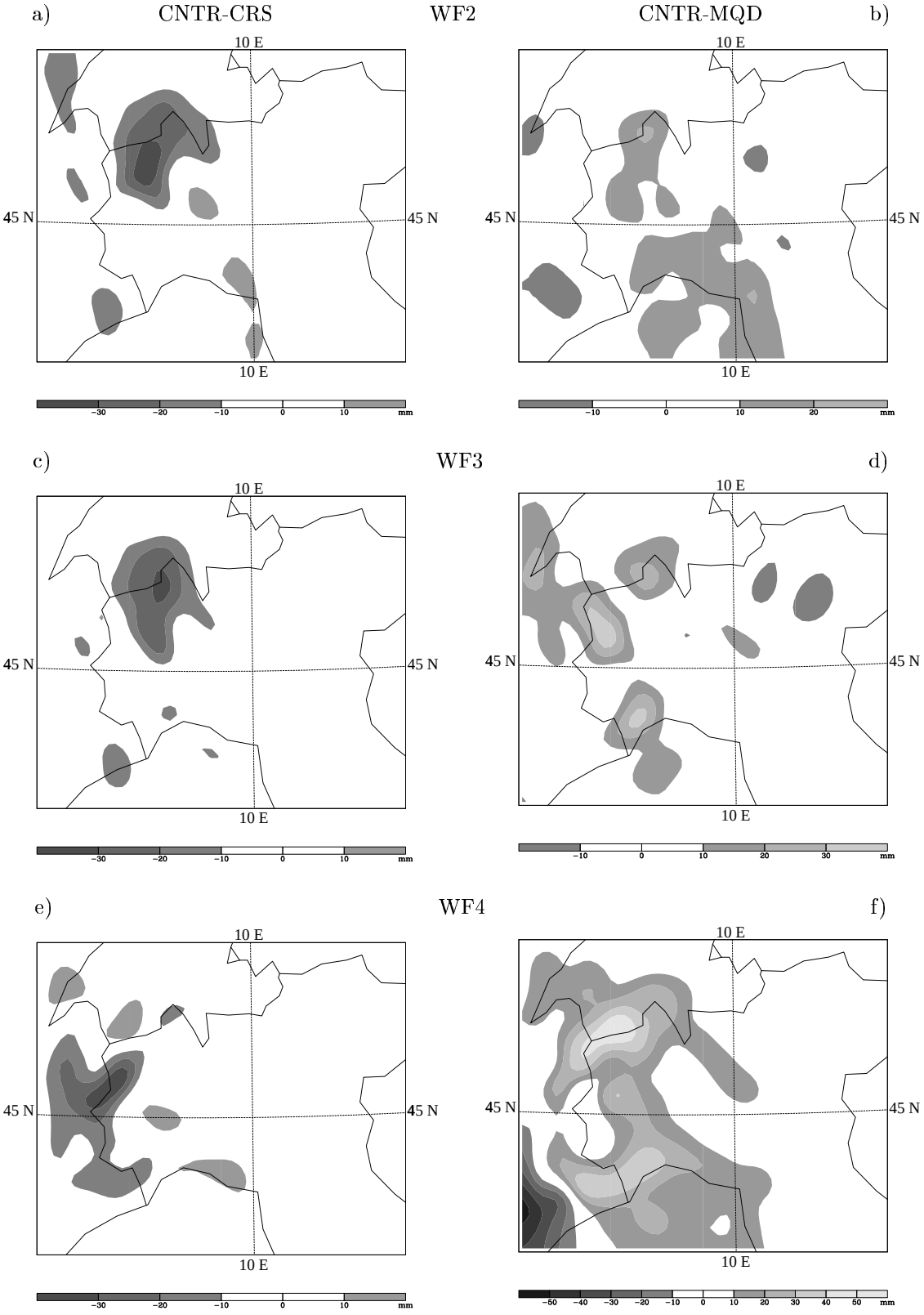

Figure 18. As in figure 17, but for domain 2.

a) WF8

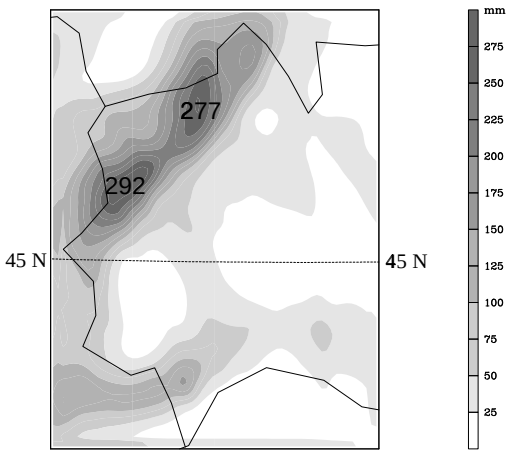

b) CNTR-WF9 (CRS)

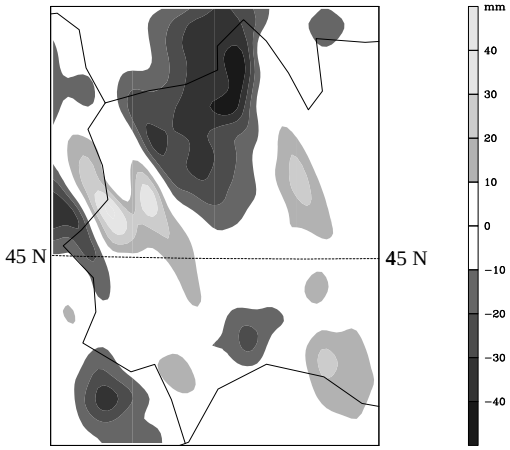

c) CNTR-WF9 (MQD)

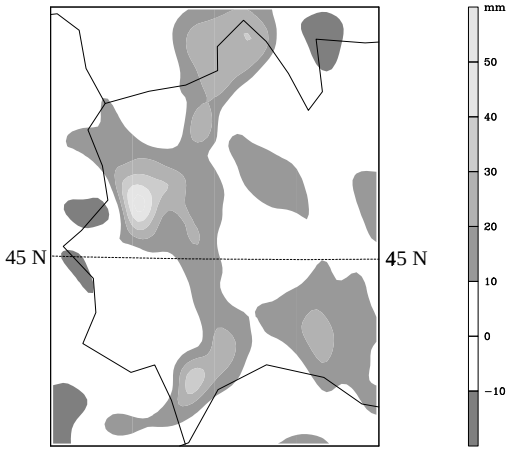

Figure 19. 24h accumulated precipitation ending at 0600 UTC 6 Nov 1994 on the innermost domain for a) CNTR. The contours interval are of 50 mm between 50 and 350 mm. Differences between CNTR and b) WF9-CRS, c) WF9-MQD 24h accumulated precipitations ending at 0600 6 UTC Nov 1994.

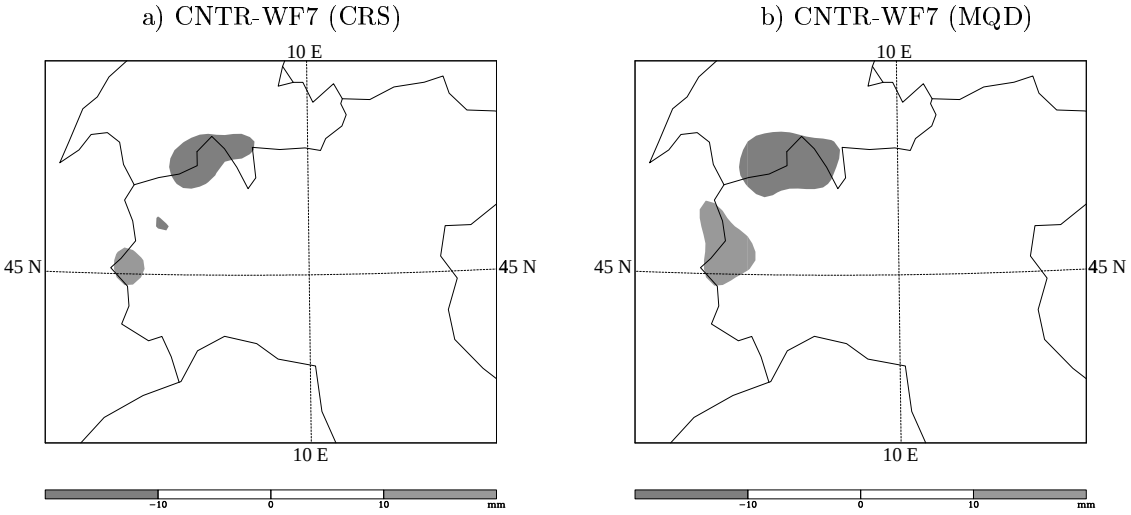

Figure 20. Differences between CNTR and a) WF7-CRS, b) WF7-MQD 24h accumulated precipitations ending at 0600 UTC 6 Nov 1994. OA is applied to the I.C. only.

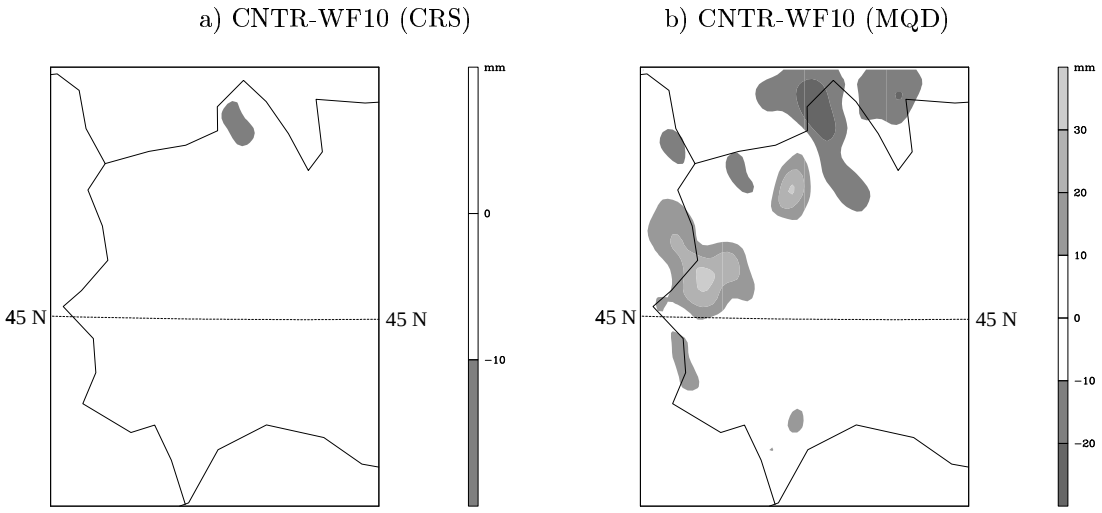

Figure 21. As in figure 20, but for experiment WF10 on the third domain.